JOURNAL OF MATERIALS SCIENCE 28 (1993) 4143–4152

Stress analysis of elastomeric materials at large extensions using the finite element method

Part I *Stress and strain distribution around spherical holes*

Y. FUKAHORI, W. SEKI
Research and Development Division, Bridgestone Corporation, Kodaira-shi, Tokyo 187, Japan

The finite element analysis newly developed is applied to stress and strain analyses around spherical holes in elastomers from small to very large deformations. The stress and strain distributions computed based on the strain-energy function of real elastomers measured through strip-biaxial testing agree well with the classical theoretical ones at small strain. At large extension, however, the maximum stress concentration factor increases and the maximum strain concentration factor decreases as strain increases. These tendencies will be increased more in carbon black-filled elastomers than in unfilled ones. The successful description for these phenomena can be achieved by mainly considering the non-linear properties in the stress–strain relation of elastomers which increase as extension increases and carbon black content increases.

1. Introduction

The phenomenon of failure by catastrophic crack propagation in structural materials poses many problems in design and analysis in fields of engineering. The driving needs for methods which quantify the effects of the presence of stress raisers on material performance have led to the evolution and development of the fracture theories. Stress raisers such as cavity, crack and rigid spheres are present to some degree in all structures. They may exist as basic defects in the constituent materials or they may be induced in construction or during service life. Therefore, it is a fundamental requirement in fracture theories, particularly in the fracture mechanics theory, to quantify the effects of stress raisers on material performances based on accurate knowledge of the stress field in the vicinity of the stress raiser for structural geometry and loading and boundary conditions in question. Many systematic stress analyses have been carried out theoretically, experimentally and numerically in metals and plastics, whose data, as is well known, have played quite important roles for structural design and fracture analysis of these materials.

Unfortunately, however, in elastomeric materials it seems to be rarely the case for stress anslysis to be performed, except for a few experimental results reported by Thomas [1], Andrews [2], Knauss [3], Fukahori [4] and Andrews and Fukahori [5]. They all showed that the stress concentration around an edge crack along the crack axis is roughly expressible in a form which is similar to that derived from classical elasticity theory even when a rubber sheet containing the crack is largely extended. However, these experiments give only a rough solution for selected, relatively simple cases in geometries and loading conditions and of course, do not give any general and accurate solution for stress analysis of elastomeric materials undergoing large deformation.

One of the most serious reasons why stress analysis has not been widely carried out for elastomeric materials seems to be attributable to the fact that elastomer study remains terribly backward in numerical techniques such as finite element and boundary integral methods. As is well known, because a finite element method (FEM) is based originally on classical or small strain, linear elasticity theory, there exist several difficulties which have to be overcome for the application of FEM to elastomers, concerning non-linear stress–strain relations and incompressible behaviour of the elastomer, in addition to its tremendous amount of deformation (over several hundred per cent to failure).

It was Rivlin [6] who developed a mathematical theory of elasticity based on the strain-energy function for large deformation behaviour of non-linear rubber-like materials, which made possible a finite element analysis in elastomers under large deformation. The first trial was performed by Lindley [7, 8], in which he analysed the stress concentration around a circular hole in a stretched rubber sheet (plane stress condition). Although his numerical treatment could manage the stress analysis of rubber at moderately large deformation, there were some problems in the strain-energy function he used, which is based on the Gent–Thomas equation (see Section 2.2).

After detailed experiments of Kawabata *et al.* [9] and Fukahori and Seki [10], concerning the strain-energy function of elastomers, Fukahori and co-

0022–2461

workers [11, 12] established a quantitative numerical method, a large deformation finite element method, by comparing in detail their experiments and numerical results for largely deformed rubber and rubber products in one-, two- and three-dimensional conditions, which showed a very good agreement between experiments and computations. The employed the strain-energy functions of elastomers obtained experimentally with a newly developed strip-biaxial machine and combined these data with the computer program. There is little published information on stress analysis in elastomers, in particular those evaluated with a finite element analysis, except for only a few cases as described earlier.

In this report the numerical method [11, 12] is applied to stress and strain analyses around a spherical hole (cavity) in elastomers from small to very large deformation near their fracture and quantitative and systematic answers are given to the following questions compared with classical elasticity solutions.

1. Do the numerical results performed at large extension agree with the classical solution in the stress and strain distribution around a spherical cavity?
2. If there is no agreement between them, how do the stress and strain distributions vary with the strain amplitude?
3. What is the point of characterizing the stress and strain distribution under large deformation in elastomers?

2. Theoretical background

2.1. Stress concentration around a spherical hole

According to the classical elasticity theory [13, 14], the stresses around a spherical hole represented in terms of the polar coordinate system (Fig. 1) are given by the following equations when the system is subjected to a uniform stress, σ_o, in the z direction at $r = \infty$;

$$\sigma_{rr} = 2E\left[\frac{2A}{r^3} - \frac{2\nu}{1-2\nu}\frac{C}{r^3} + 12\frac{B}{r^5} + \left(-\frac{2(5-\nu)}{1-2\nu}\frac{C}{r^3} + 36\frac{B}{r^5}\right)\cos 2\theta\right] + \sigma_o\cos^2\theta \quad (1)$$

$$\sigma_{\theta\theta} = 2E\left[-\frac{2A}{r^3} - \frac{2\nu}{1-2\nu}\frac{C}{r^3} - 3\frac{B}{r^5} + \left(\frac{C}{r^3} - 21\frac{B}{r^5}\right)\cos 2\theta\right] + \sigma_o\sin^2\theta \quad (2)$$

$$\sigma_{\varphi\varphi} = 2E\left[-\frac{2A}{r^3} - \frac{2(1-\nu)}{1-2\nu}\frac{C}{r^3} - 9\frac{B}{r^5} + \left(3\frac{C}{r^3} - 15\frac{B}{r^5}\right)\cos 2\theta\right] \quad (3)$$

$$\sigma_{r\theta} = 2E\left[-\frac{2(1+\nu)}{1-2\nu}\frac{C}{r^3} + \frac{B}{r^5}\right] \times (\sin 2\theta - \sigma_o\sin\theta\cos\theta) \quad (4)$$

$$\sigma_{r\varphi} = \sigma_{\theta\varphi} = 0 \quad (5)$$

where the values of A, B and C are constants and are given by

$$A = \frac{r_o^3\sigma_o}{8E}\frac{13-10\nu}{7-5\nu}$$

$$B = \frac{r_o^5\sigma_o}{8E}\frac{1}{7-5\nu}$$

$$C = \frac{r_o^3\sigma_o}{8E}\frac{1}{8-10\nu}$$

and r_o is the radius of a spherical hole, E is Young's modulus and ν is Poisson's ratio of the material. The corresponding strains are also given by

$$\varepsilon_{ii} = \frac{\sigma_{ii}}{E} - \sum_{i\neq j}\frac{\nu\sigma_{jj}}{E} \quad (6)$$

$$\varepsilon_{ij} = \frac{2(1+\nu)\sigma_{ij}}{E} \quad (i \neq j) \quad (7)$$

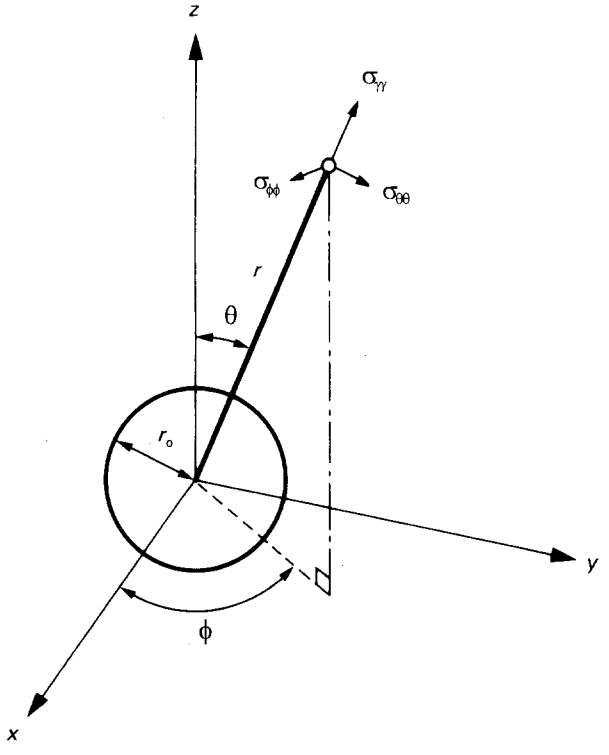

Figure 1 The polar coordinate system.

2.2. Strain-energy function

Stress–strain relations of homogeneous, isotropic and elastic materials can be derived from the strain-energy function, W, the elastic energy stored in a deformed body. According to Rivlin [6], the strain-energy function, W, is given as a function of strain invariants I_1, I_2 and I_3

$$W = W(I_1, I_2, I_3) \quad (8)$$

where $I_1 = \lambda_1^2 + \lambda_2^2 + \lambda_3^2$, $I_2 = \lambda_1^2\lambda_2^2 + \lambda_2^2\lambda_3^2 + \lambda_3^2\lambda_1^2$, $I_3 = \lambda_1^2\lambda_2^2\lambda_3^2$ and λ_1, λ_2 and λ_3 are the principal extension ratios. In general, $I_3 = 1$ because of the incompressibility of rubber.

In a homogeneous biaxial deformation, the principal stress (engineering stress) σ_1 and σ_2 are derived from W [15],

$$\sigma_1 = \frac{2}{\lambda_1}\left(\lambda_1^2 - \frac{1}{\lambda_1^2\lambda_2^2}\right)\left(\frac{\partial W}{\partial I_1} + \lambda_2^2\frac{\partial W}{\partial I_2}\right) \quad (9)$$

$$\sigma_2 = \frac{2}{\lambda_2}\left(\lambda_2^2 - \frac{1}{\lambda_1^2\lambda_2^2}\right)\left(\frac{\partial W}{\partial I_1} + \lambda_1^2\frac{\partial W}{\partial I_2}\right) \quad (10)$$

Then $\partial W/\partial I_1$ and $\partial W/\partial I_2$ can be calculated by substituting the data sets of σ_1, σ_2, and the corresponding λ_1, λ_2 obtained through biaxial experiments into the following equations derived from Equations 9 and 10

$$\frac{\partial W}{\partial I_1} = \frac{1}{2(\lambda_1^2 - \lambda_2^2)}\left(\frac{\lambda_1^3\sigma_1}{\lambda_1^2 - \lambda_1^{-2}\lambda_2^{-2}} - \frac{\lambda_2^3\sigma_2}{\lambda_2^2 - \lambda_1^{-2}\lambda_2^{-2}}\right) \quad (11)$$

$$\frac{\partial W}{\partial I_2} = \frac{1}{2(\lambda_2^2 - \lambda_1^2)}\left(\frac{\lambda_1\sigma_1}{\lambda_1^2 - \lambda_1^{-2}\lambda_2^{-2}} - \frac{\lambda_2\sigma_2}{\lambda_2^2 - \lambda_1^{-2}\lambda_2^{-2}}\right) \quad (12)$$

In the case of uniaxial extension, considering $\lambda_2 = \lambda_1^{-1/2}$

$$\sigma = 2(\lambda - \lambda^{-2})\left(\frac{\partial W}{\partial I_1} + \lambda^{-1}\frac{\partial W}{\partial I_2}\right) \quad (13)$$

In Equation 13, a neo-Hookean material which gives a linear rubber elasticity is a special case when $\partial W/\partial I_1$ is constant and $\partial W/\partial I_2 = 0$. On the other hand, the Mooney material corresponds to the case where both of $\partial W/\partial I_1$ and $\partial W/\partial I_2$ are constant, which is the simplest description for a non-linear elastomeric material.

Because Equation 13 also includes two unknown parameters, $\partial W/\partial I_1$ and $\partial W/\partial I_2$, it is fundamentally impossible to decide these two parameters with a single equation, in other words with a simple extension test. As Kawabata *et al.* [9] and Fukahori and co-workers [10, 12] showed experimentally, $\partial W/\partial I_1$ and $\partial W/\partial I_2$ are not constant but are complicated functions of I_1 and I_2 and thus λ_1 and λ_2. Therefore the treatments proposed by Rivlin and Saunders [16] the so-called Mooney–Rivlin and Gent–Thomas [17] plots, both of which assume two constants as a premise for $\partial W/\partial I_1$ and $\partial W/\partial I_2$ given by a simple extension test, are not valid for representing the general form of the strain-energy function [10]. That is, the strain-energy function obtained through a simple extension test is valid only for the stress–strain behaviour in simple extension.

2.3. Finite element method

The incompressible condition is important for a finite element analysis of rubber-like materials. The present work is based on the Lagrange multiplier method for incompressible constraint proposed by Oden [18], where the strain-energy function, W, is replaced by

$$\tilde{W} = W(I_1, I_2) + \frac{P}{2}(I_3 - 1) \quad (14)$$

where P is the Lagrange multiplier of the constraint, which is a hydrostatic pressure independently derived from the displacement field and directly related to the bulk modulus. Then, a constitutive equation for incompressible rubber can be written as a relation between the second Piola–Kirchhoff stress tensor S_{ij}, the Green–Lagrange strain and deformation tensor E_{ij} and C_{ij} and hydrostatic pressure, P

$$S_{ij} = \frac{\partial W}{\partial E_{ij}} = 2\left[\frac{\partial \tilde{W}}{\partial I_1}\delta_{ij} + \frac{\partial W}{\partial I_2} \times (I_1\delta_{ij} - C_{ij})\right] + P(C_{ij})^{-1} \quad (15)$$

Now consider the total energy function $\pi(u, P)$ given by Equation 16

$$\pi(u, P) = \int \tilde{W} dv - F(u) \quad (16)$$

where $F(u)$ is a potential energy of external force and v is a volume of the undeformed configuration. According to the principle of the virtual work, the function π has a minimum value in its equilibrium condition. Thus, we can obtain the formulation, the so-called mixed or hybrid method for the incompressibility problem, which is a generalization of Hermann's variational principle. The computer program predominantly used in this report is MARC, with subroutines modified where necessary.

3. Experiments and numerical treatments

3.1. Apparatus and materials

A summary of the new apparatus to perform strip-biaxial (pure shear) testing which was introduced in detail elsewhere [10], as shown in Fig. 2, is now given. The rectangular test piece can be extended freely in the x-direction, while in the y-direction, the test piece is kept constant ($\lambda_2 = 1$) gripped in sliding clamps. Thus, data from σ_1 and σ_2 measured by paired load cells connected to fixed crossheads make calculations of $\partial W/\partial I_1$ and $\partial W/\partial I_2$ from Equations 11 and 12 possible. In this research, we used the following types of empirical equation for $\partial W/\partial I_1$ and $\partial W/\partial I_2$ by a least-squares method

$$\frac{\partial W}{\partial I_i} = a_i + b_i(I_i - 3) + c_i(I_i - 3)^2 + d_i \exp[e_i(I_i - 3)] \quad (17)$$

The materials used here were unfilled (NR1), slightly filled (NR2) and heavily filled (NR3) natural rubber vulcanizates with carbon black. The relevant compounding recipes are given in Table I. NR2 was mostly used for computation, unless noted otherwise.

3.2. Stress–strain relations

Stress–strain curves in simple extension for three rubber vulcanizates are shown in Fig. 3, while the values of $\partial W/\partial I_1$ and $\partial W/\partial I_2$ obtained in a strip-biaxial testing are plotted against strain in Fig. 4. As indicated earlier, $\partial W/\partial I_1$ and $\partial W/\partial I_2$ are not constant but have typical features varying with I_1 and strain. More or

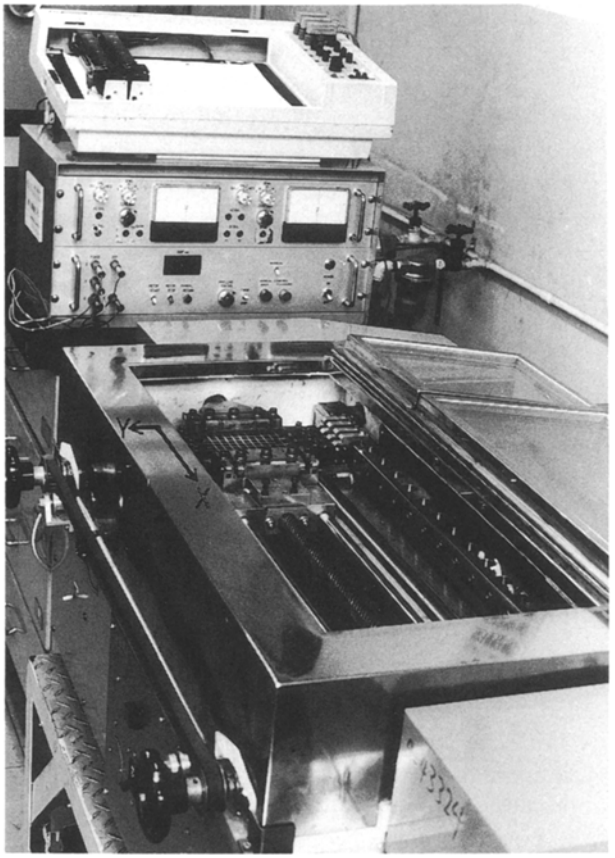

Figure 2 The strip-biaxial testing machine.

TABLE I Compounding details of the materials (parts by weight)

Composition	NR1	NR2	NR3
Rubber	100 (NR)	–	–
Carbon black	0	25 (FT)	60 (HAF)
Sulphur	0.7	1.5	2.0

In addition, zinc oxide (5.0) and steric acid (2.0) for all rubbers and aromatic oil (9.0) for NR2 only.

less, all rubber vulcanizates, of any rubber species and whether filled or unfilled have similar features [10] to Fig. 4.

3.3. The numerical model

Spherical inclusions randomly distributed in an infinite matrix can be represented by a cylinder of matrix containing a single sphere of a radius r_o at its centre, its radius R_o and the height $2R_o$, in a finite element analysis, as shown in Fig. 5. The cylinder can be predicted by the plane ABCDEF using axisymmetric elements, the z-axis being the axis of symmetry. The boundary conditions which must be satisfied in the calculation are as follows (shown in Fig. 6).

1. The stresses do not work on the boundary of the sphere, $\sigma_{rr} = \sigma_{r\theta} = 0$, which means that the sphere can deform freely at its interface;

2. no constraint is imposed on the side surface of the cylinder, i.e. free deformation and no external force;

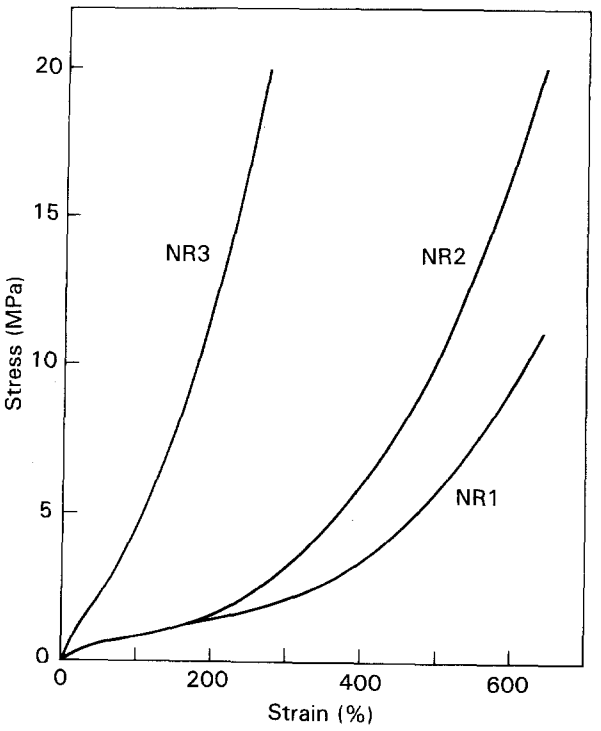

Figure 3 Stress–strain relations in simple extension.

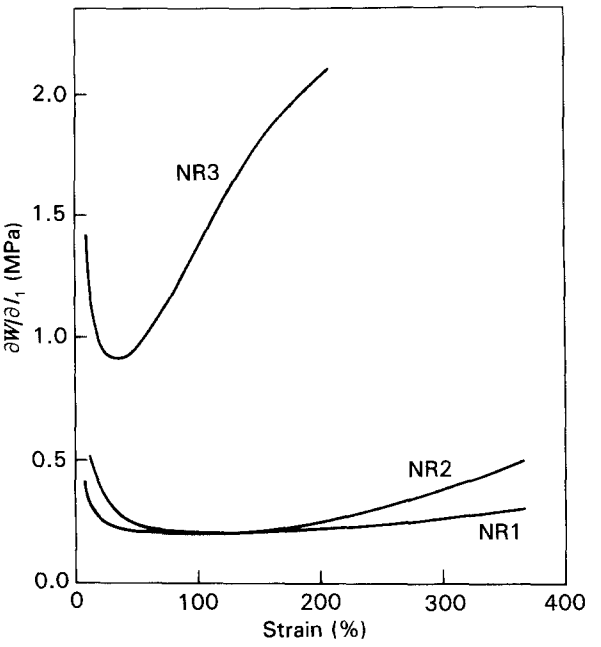

Figure 4 $\partial W/\partial I_1$ as a function of strain.

3. the circular surface of the cylinder is constrained to remain perpendicular to the z-axis, but freely deformable in the x-direction.

The deformation of the grid is achieved by loading the grid (a uniform stress, σ_o) by prescribed displacement in the z-direction.

The volume fraction, V, of spheres which occupy the system can be calculated by the relation, $v = 2/3\ (r_o/R_o)^3$. An increase in the value of the geometrical parameter r_o/R_o is equivalent to the holes being close together. In the present computation, the radius of the phere, r_o, was kept constant, while that of the cylinder was varied, the relation between the geometric parameter, r_o/R_o, and volume fraction, v, being as given in

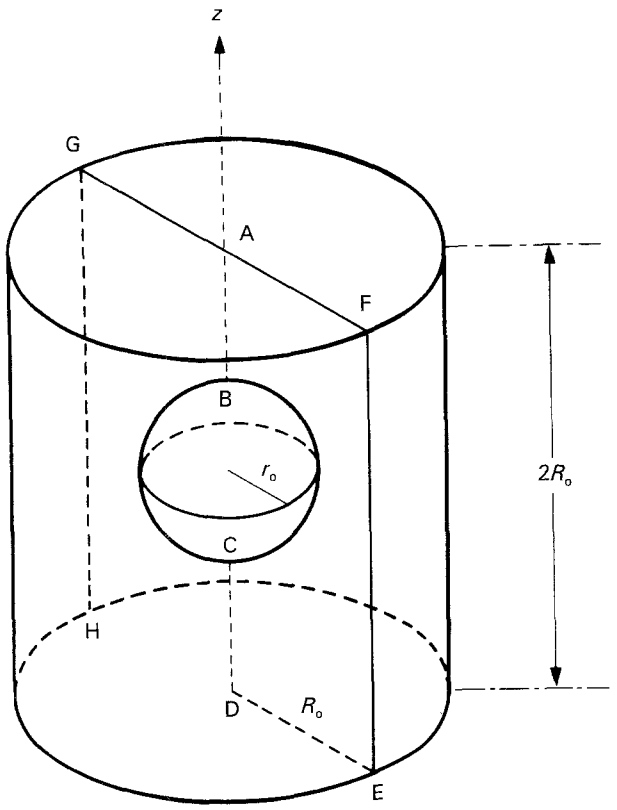

Figure 5 A cylinder of matrix containing a single sphere at its centre.

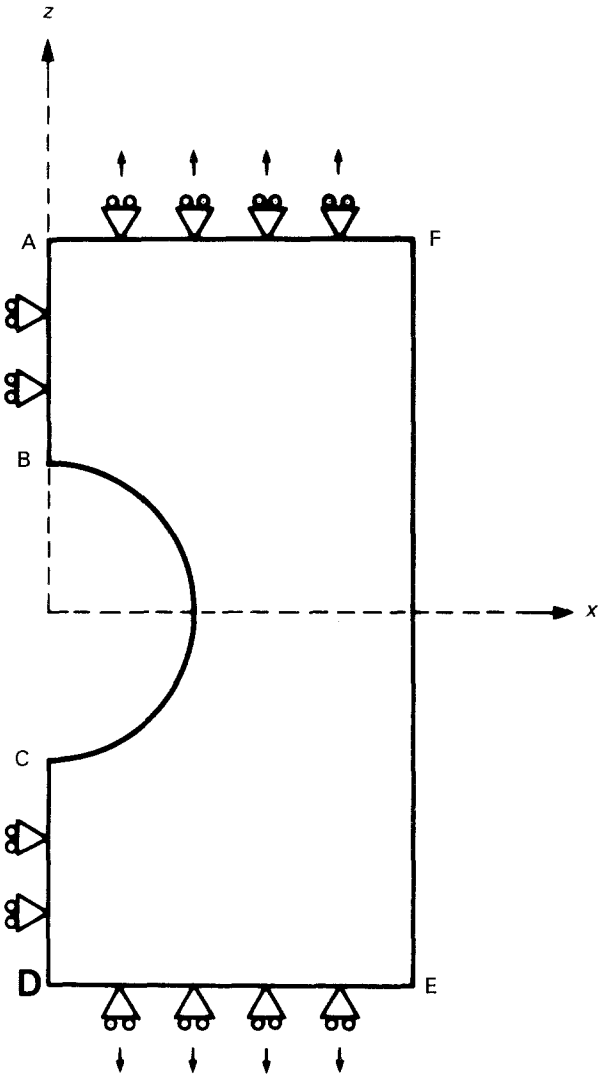

Figure 6 The plane ABCDEF given in Fig. 5 using axisymmetric elements, the z-axis being the axis of symmetry.

Table II. Fig. 7 represents the typical finite element model for the computation, in which only a quarter of the map is shown.

The computation gives the maximum principal stress (true stress), σ, and the maximum principal strain, ε. Uniform (average) stress applied to the system, σ_0 is calculated from the sum of force applied to the circular surface of the cylinder divided by its surface area. All stress and strain fields are represented by the stress concentration factor $\alpha(= \sigma/\sigma_0)$ and strain concentration factor $\beta(= \varepsilon/\varepsilon_0)$ and the maximum stress and strain concentration factors, α_{max} and β_{max}, respectively.

TABLE II Relation between the geometric parameter, r_0/R_0, and volume fraction, v

r_0/R_0	v (%)
1/12	3.85×10^{-2}
1/5	5.33×10^{-1}
1/2	8.33
1/1.5	1.98×10
1/1.2	3.85×10

4. Results

4.1. Stress and strain distribution around a spherical hole subjected to uniaxial tensile stress

Figs 8 and 9 give contour maps of stress concentration factor, α, and strain concentration factor, β, around a spherical hole represented on the undeformed coordinates computed at small average strain ($\varepsilon_0 = 10\%$) and $r_0/R_0 = 1/12$, in whose condition the disturbance for stress and strain distribution around a hole by adjacent holes can be neglected. Fig. 8 shows the distribution of α at any point around a hole. The maximum concentration appears along the x-axis at $r = r_0$, the boundary of the hole and its absolute value is 2.12, which is slightly smaller than the theoretical value, $\alpha_{max} = 2.16$. The maximum strain concentration occurs at the same position that α_{max} appears and its value is 1.88, which is also slightly smaller than the theoretical value, $\beta_{max} = 1.92$. These small disagreements between the computation and theory come from making a coarse mesh in computation and are not essential discrepancies. Anyway it is clearly seen that the stress and strain distribution and their absolute values around a spherical hole computed based on the strain-energy function obtained empirically at small strain agree well with ones theoretically calculated using the classical elasticity solution, Equations 1–5, and Equations 6 and 7 when $\nu = 0.5$.

On the other hand, at very large deformation, however, the computed contour maps give different features. Figs 10 and 11 are contour maps of α and β, respectively, computed at very large average strain ($\varepsilon_0 = 300\%$) and $r_0/R_0 = 1/12$. The maximum concentration factor, α_{max}, becomes considerably larger than

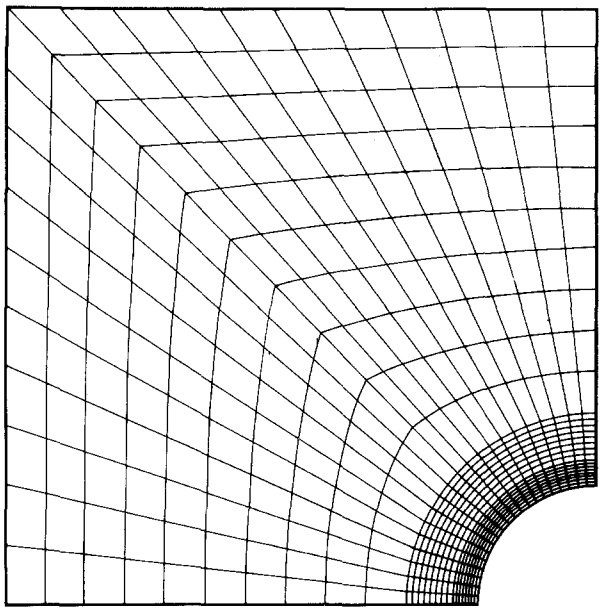

Figure 7 Finite element grid with axisymmetric elements.

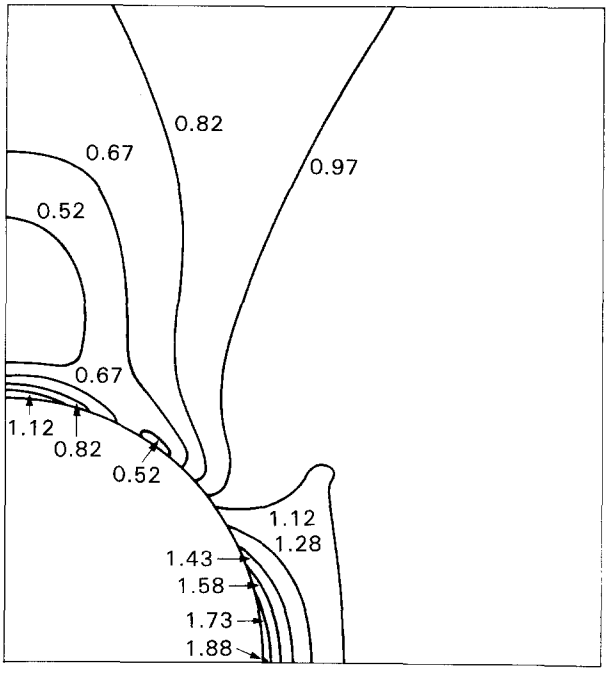

Figure 9 As Fig. 8, but of strain concentration factor, β.

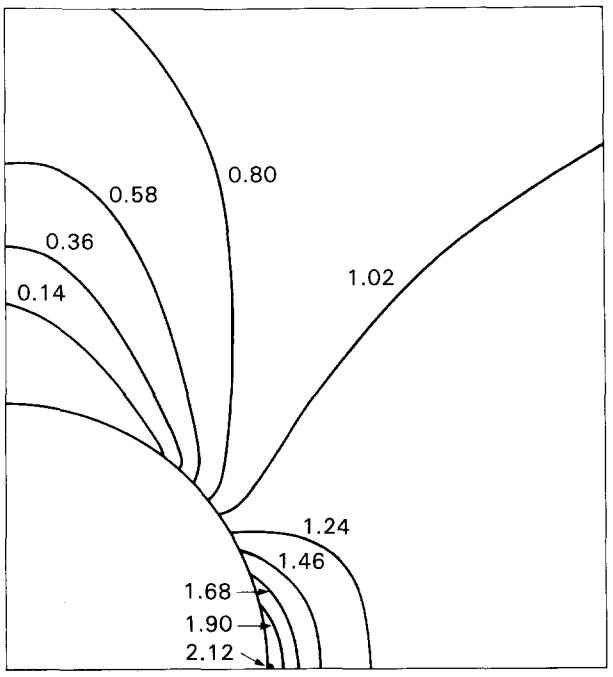

Figure 8 Contour maps of stress concentration factor, α, around a spherical hole represented on the undeformed coordinates at $\varepsilon_0 = 10\%$ and $r_0/R_0 = 1/12$.

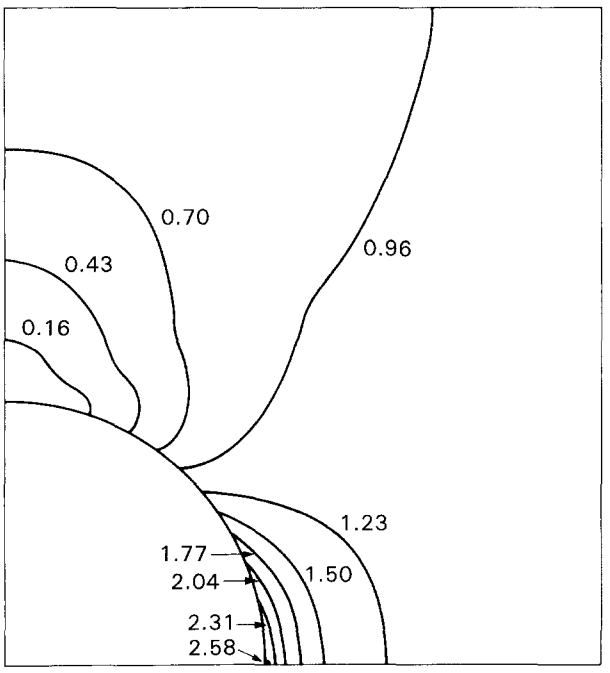

Figure 10 As Fig. 8, but at $\varepsilon_0 = 300\%$ and $r_0/R_0 = 1/12$.

the calculated one, that is $\alpha_{max} = 2.58$, as shown in Fig. 10. On the contrary, β_{max} is much smaller than the calculated one, i.e. $\beta_{max} = 1.40$ (Fig. 11).

These situations are understood more clearly by plotting α and β against the distance from the surface of the cavity along the x-axis. The distribution of α is plotted as a function of r/r_0 at various average strains along the x-axis in Fig. 12. When an average strain is less than 10%, the α–r/r_0 curve completely makes a good fitting with the theoretical one. However, as an average strain increases, the α–r/r_0 curve shows the rapid increase of α at a small distance r, which produces the higher value of α_{max} at the boundary of a hole. However, in the case of the distribution of β, the situation will be reversed, except the case that the β–r/r_0curve at small average strain ($\varepsilon_0 = 10\%$) also makes a good fitting with the theoretical curve. That is, in the β–r/r_0 curve, the upturn of β at a small distance from the boundary of a hole will diminish and as a result β_{max} decreases rapidly with increasing average strain, as shown in Fig. 13. Therefore, we can conclude that stress and strain distribution around a spherical hole deviate from those given by the theoretical solution as average strain increases, which re-

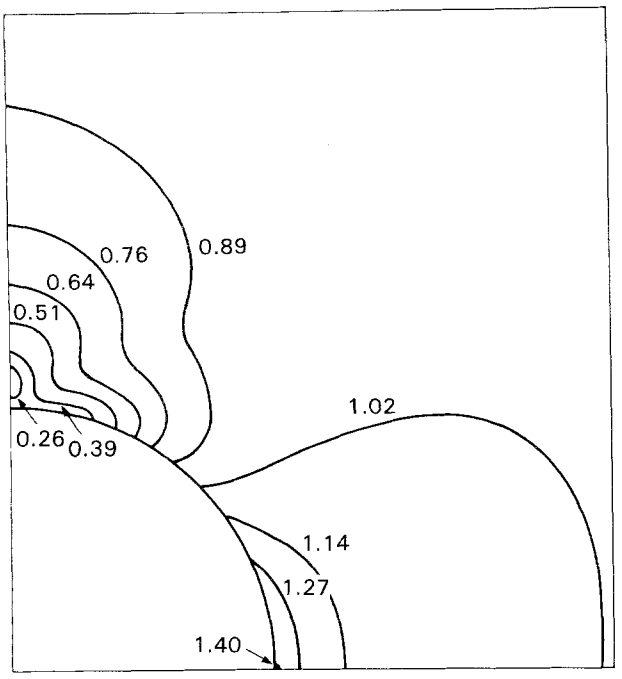

Figure 11 As Fig. 9, but at $\varepsilon_o = 300\%$ and $r_o/R_o = 1/12$.

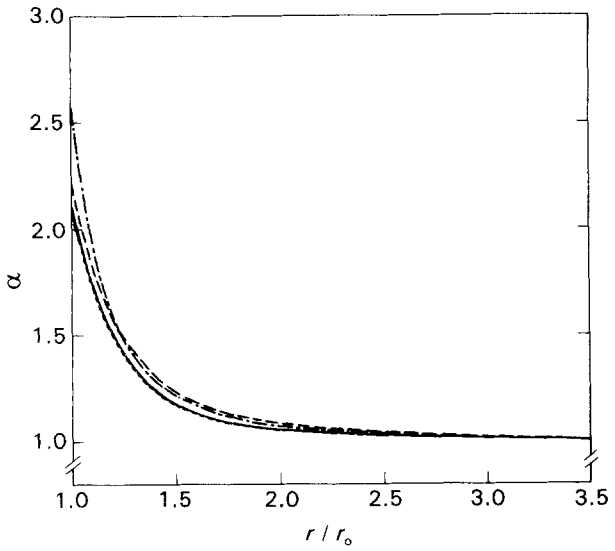

Figure 12 Stress concentration factor as a function of r/r_o along the x-axis. ε_o: (— · —) 300%, (— — —) 100%, (——) 10%, (- - -) theoretical.

sults in a larger value in α_{max} and a smaller value in β_{max} with increasing average strain compared with classical theory.

4.2. Influence of adjacent holes on stress and strain distribution around a spherical hole

The distribution of α and β around a spherical hole are significantly disturbed by the presence of adjacent holes. Figs 14 and 15 are contour maps of α and β at small average strain ($\varepsilon_o = 10\%$) when other adjacent holes are close to the hole, i.e. the geometrical parameter $r_o/R_o = 2/3$. The characteristic high value of α_{max} is seen in Fig. 14, whereas β_{max} does not change much, as shown in Fig. 15. These situations are clearly

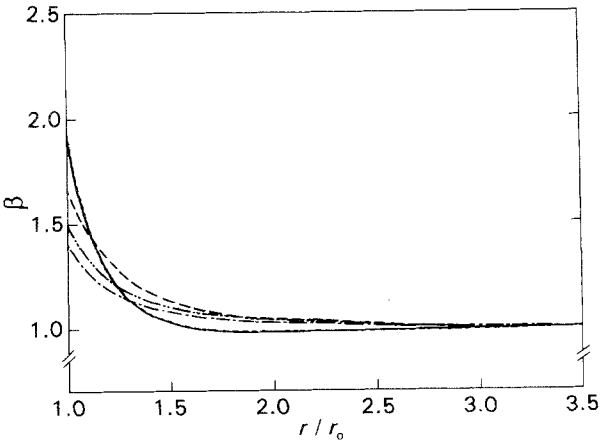

Figure 13 Strain concentration factor as a function of r/r_o along the x-axis. ε_o: (— · —) 300%, (— — —) 200%, (— - - —) 100%, (——) 10%, (- - -) theoretical.

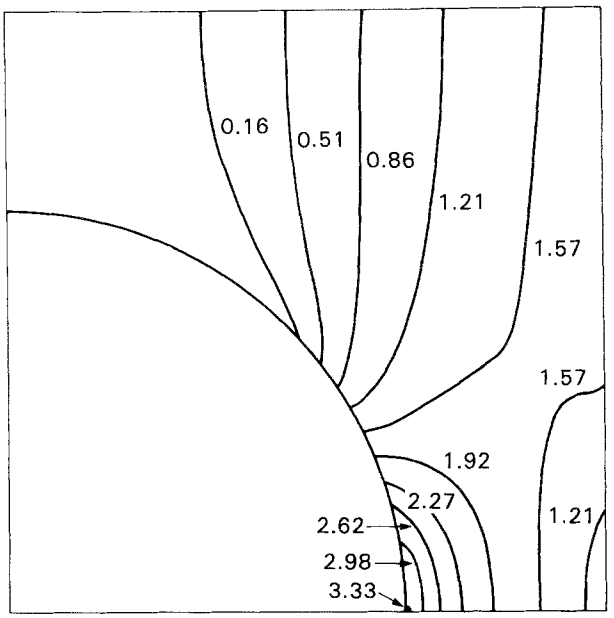

Figure 14 Contour maps of α around a spherical hole disturbed by adjacent holes, at $\varepsilon_o = 10\%$ and $r_o/R_o = 2/3$.

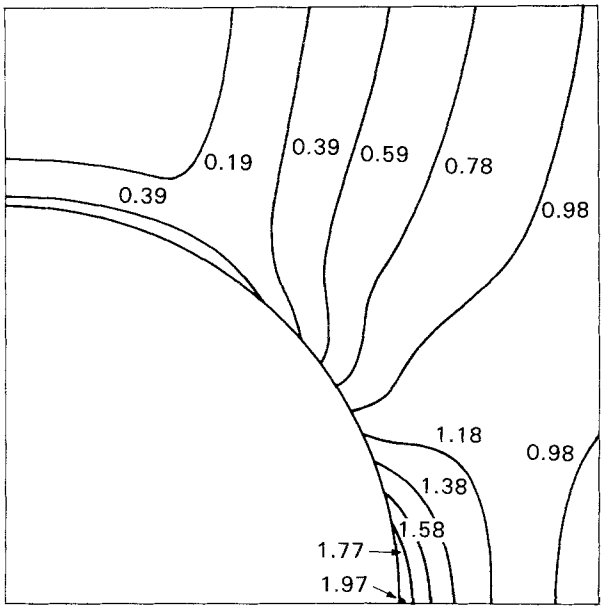

Figure 15 As in Fig. 14, but of β.

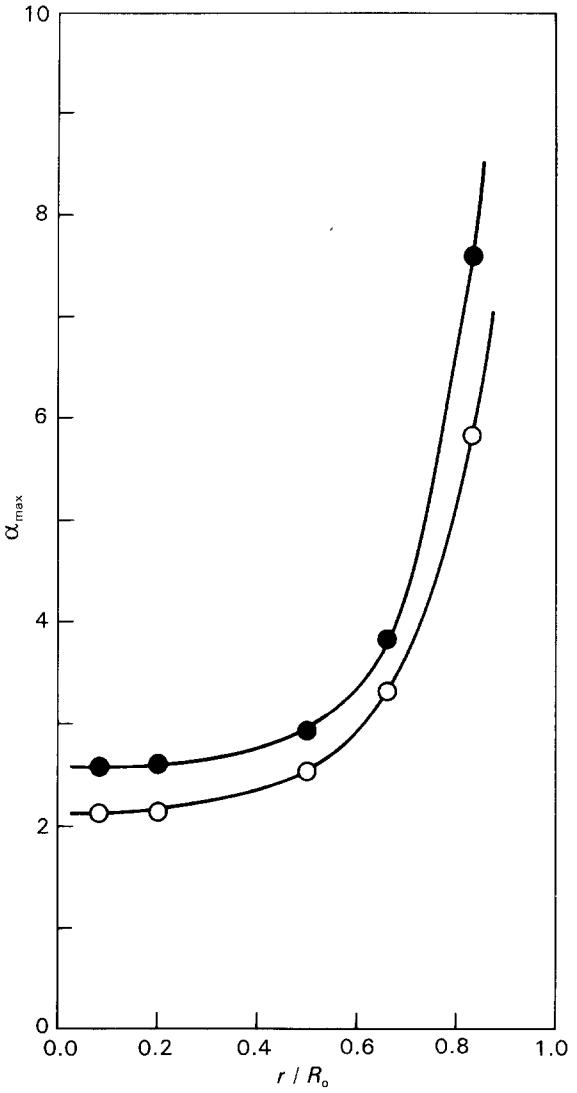

Figure 16 α_{max} as a function of r_o/R_o. ε_o: (●) 300%, (○) 10%.

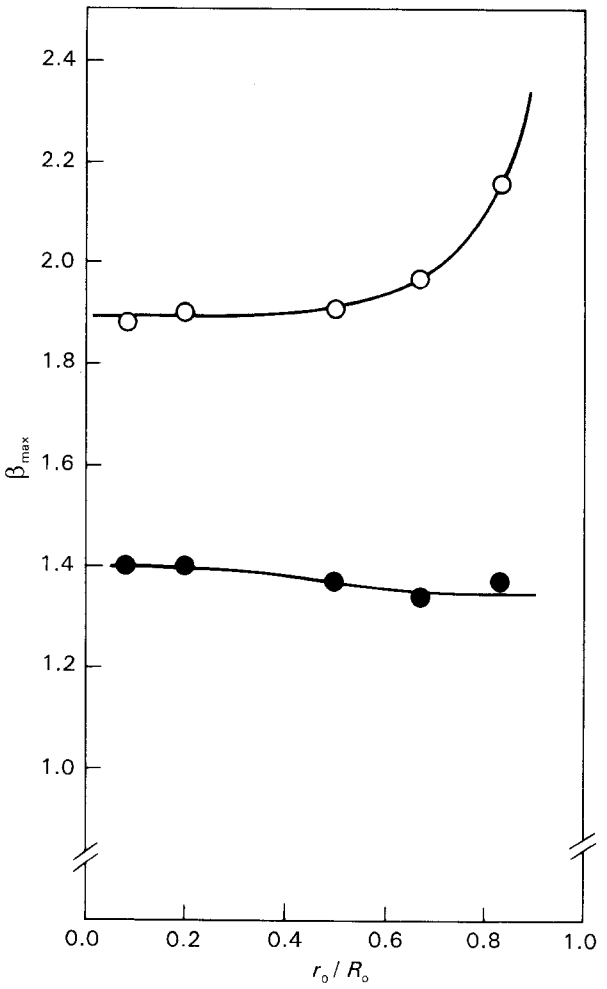

Figure 17 β_{max} as a function of r_o/R_o. ε_o: (●) 300%, (○) 10%.

illustrated in Figs 16 and 17. Fig. 16 is the relation between α_{max} and r_o/R_o and indicates that α_{max} increases gradually in a region of the small value of r_o/R_o but increases greatly when the value of r_o/R_o exceeds around 0.5 as r_o/R_o increases. However, on the other hand, β_{max} is not influenced so much by the presence of adjacent holes, as shown Fig. 17. Anyway, it is shown that in any cases of different values of r_o/R_o, α_{max} at large extension is always larger than that at small extension and β_{max} at large extension is always smaller than that at small extension.

5. Discussion

Now we consider the reason why α_{max} increases and β_{max} decreases in elastomeric materials as the average uniform strain increases. Needless to say, the classical theoretical solution is given under the assumption of linear elasticity and infinitesimal strain. Therefore, when we treat the problems of large deformation in elastomeric material, we must take geometric and material non-linearity into consideration, in which both effects may generally be combined together. For the question of non-linearities arising from geometry of structures, Yang [19] gave a good clue to consider the large deformation of rubbers. In his theoretical treatment, he calculated the stress and strain concentration factors under moderately large deformation for a circular rubber sheet with a centred circular hole and rigid circular inclusion, the plane-stress assumption being considered, using the strain-energy function of the so-called Mooney-type material. Although the Mooney material is different from a neo-Hookean material, we may virtually ignore the difference in both materials, as long as a strain is not so large, less than 100%, for instance. The results thus calculated show that for a circular hole, the maximum stress concentration factor increases greatly and the maximum strain concentration factor increases slightly as an average strain increases, due to the effect of large change in geometry.

Now we consider our numerical results for real elastomeric materials compared with the calculated results for the Mooney material [19]. Fig. 18 gives α_{max} computed as a function of average strain, ε_o, at $r_o/R_o = 1/12$ for three rubber vulcanizates, NR1 (unfilled), NR2 (slightly filled) and NR3 (heavily filled). As mentioned earlier, the characteristic stress–strain relation and relation between $\partial W/\partial I_1$ and λ_1 in elastomeric materials strongly depend on filler contents, the more filled, the more non-linear the relations, as shown in Figs 3 and 4. That is, the stress gradually deviates from the linear stress–strain relation as strain increases. In Fig. 18, it is shown that values of α_{max} for three elastomeric materials increase with increasing

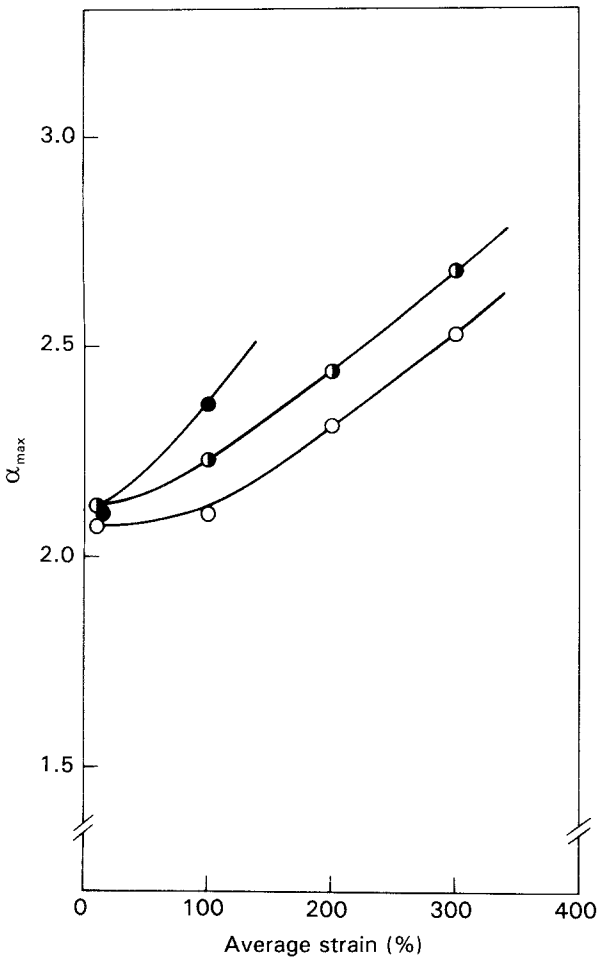

Figure 18 α_{max} as a function of strain for various rubber vulcanizates: (○) NR1, (◑) NR2, (●) NR3.

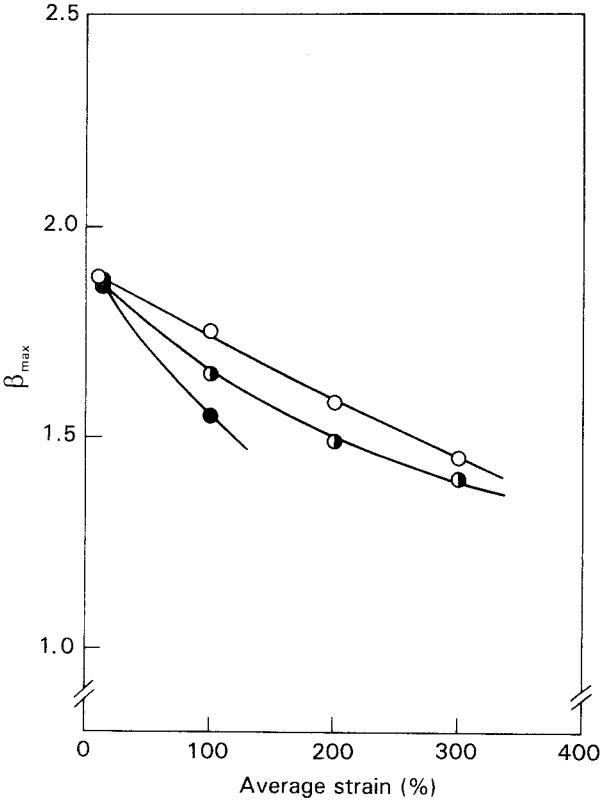

Figure 19 β_{max} as a function of strain. (○) NR1, (◑) NR2, (●) NR3.

strain amplitude, and the more filled, the more increased is α_{max}. Considering that even an unfilled rubber shows material non-linearity to some extent, as shown in Figs 3 and 4, both geometric and material non-linearity obviously play an important role in the deviation of α_{max} given by numerical analysis at large extension from the classical (infinitesimal strain) theoretical solution. We can say, however, that a more important contribution to the discrepancy may be attributable to the material non-linearity in elastomers.

This is shown more clearly in the case of β_{max} for three rubber vulcanizates, as plotted against average strain in Fig. 19. Although β_{max} increases slightly as the average strain increases in the Mooney material [19], β_{max} computed for rubber vulcanizate in Fig. 19 decreases with increasing average strain and the more filled, the more decreased is its value. Therefore, considering that the increase of β_{max} cannot be interpreted with the geometric non-linearity, we can conclude that the main contribution of the increase in α_{max} and the decrease in β_{max} around a spherical hole in elastomers under large extension, results from the non-linear properties of the materials which increase as extension increases.

Now let us consider the relation between the material non-linearity and the facts that α_{max} increases and β_{max} decreases as the average strain increases in elastomeric materials. In non-linear elastomeric materials,

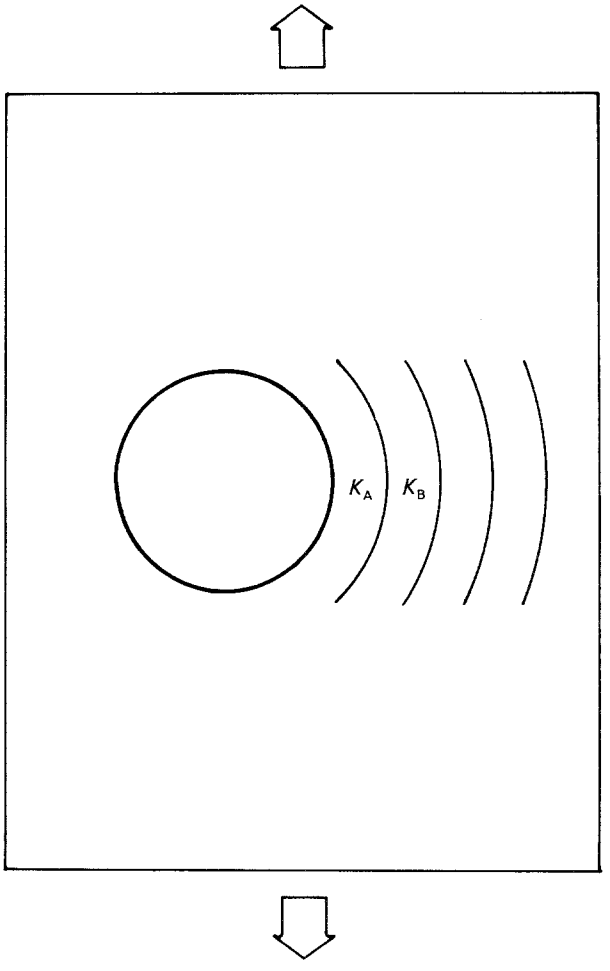

Figure 20 Schematic illustration of a hole surrounded by layers of different stiffness, K_A and K_B, $K_A > K_B$.

the stress increases by gradually deviating from the linear stress–strain relation with increasing strain, as shown in Figs 3 and 4, which means that the elastomer changes its stiffness from low to high as strain increases. Therefore, we can understand that under large extension, the elastomer component which surrounds a hole gradually increases the stiffness as it approaches the boundary of the hole. In other words, the system which surrounds a hole can be regarded as being constructed by components of different stiffness when it is highly strained. Fig. 20 gives the schematic illustration of such a situation where a hole is surrounded by layers of different stiffness, K_A and K_B, $K_A > K_B$. Now we adopt parallel and series models consisting of two springs, A and B, whose stiffness is K_A and K_B, respectively. Under uniform deformation, the stress of spring A is larger than that of spring B in the parallel model and the strain of spring A is smaller than that of spring B in the series model. Virtually, these situations must be seen in real elastomeric materials, which are well represented by the combination of two models. As a result, in non-linear materials like elastomer, the stress level of the stress-hardened component will be higher and its strain level will be lower than those of the component in linear materials when both materials are subjected to the same uniaxial load or extension. These tendencies should be more marked in carbon black-filled elastomers.

6. Conclusion

The maximum stress and strain concentration factors around a spherical hole computed using the empirical strain-energy function of elastomers agree well with the theoretical values at small average strain. At large extension, however, α_{max} increases and β_{max} decreases as the average strain increases. These tendencies will be increased more in carbon black-filled NR than in unfilled NR. These phenomena can be understood by mainly considering the non-linear properties in the stress–strain relation of elastomers which increase as extension increases and carbon black content increases.

Acknowledgement

We thank Professor S. Kawabata, Department of Polymer Chemistry, University of Kyoto, Japan, for designing the new apparatus.

References

1. A. G. THOMAS, *J. Polym. Sci.* **18** (1955) 177.
2. E. H. ANDREWS, *Proc. Phys. Soc.* **77** (1961) 483.
3. W. G. KNAUSS, *Exp. Mech.* **8** (1968) 177.
4. Y. FUKAHORI, PhD thesis, University of London (1976).
5. E. H. ANDREWS and Y. FUKAHORI, *J. Mater. Sci.* **12** (1977) 1307.
6. R. S. RIVLIN, *Philos. Trans. R. Soc.* **241** (1948) 379.
7. P. B. LINDLEY, *J. Strain Anal.* **6** (1971) 45.
8. *Idem. ibid.* **6** (1971) 279.
9. S. KAWABATA, M. MATSUDA, K. TEI and H. KAWAI, *Macromolecules* **14** (1981) 154.
10. Y. FUKAHORI and W. SEKI, *Polymer* **33** (1992) 502.
11. Y. FUKAHORI, W. SEKI, Y. ISEDA and T. MATSUNAGA, "Composites '86", Proceedings of the 3rd Japan–US Conference on Composite Materials (1986) p. 397.
12. W. SEKI, Y. FUKAHORI, Y. ISEDA and T. MATSUNAGA, *Rubb. Chem. Tech.* **60** (1987) 856.
13. J. N. GOODIER, *Trans. ASME* **55** (1933) 39.
14. S. P. TIMOSHENKO and J. N. GOODIER, "Theory of Elasticity", 3rd edn (McGraw-Hill, Kogakusha, Tokyo, 1970).
15. A. C. ERINGEN, "Nonlinear Theory of Continuous Media" (McGraw-Hill, New York, 1962).
16. R. S. RIVLIN and D. W. SAUNDERS, *Philos. Trans. R. Soc. A* **243** (1951) 251.
17. A. N. GENT and A. G. THOMAS, *J. Polym. Sci.* **28** (1958) 625.
18. J. T. ODEN, "Finite Elements of Nonlinear Continua" (McGraw-Hill, New York, 1972).
19. W. H. YANG, *J. Appl. Mech.* (1967) 942.

Received 18 May 1992
and accepted 4 January 1993